Supplement of Atmos. Chem. Phys., 25, 16589–16609, 2025 https://doi.org/10.5194/acp-25-16589-2025-supplement © Author(s) 2025. CC BY 4.0 License.





Supplement of

The transport history of African biomass burning aerosols arriving in the remote Southeast Atlantic and their impacts on cloud properties

Huihui Wu et al.

Correspondence to: Hugh Coe (hugh.coe@manchester.ac.uk)

The copyright of individual parts of the supplement might differ from the article licence.

Supplementary

5

10

15

20

25

30

S1 Observations of aerosol components and carbon monoxide

Observations of aerosol chemical compositions and carbon monoxide (CO) during the CLARIFY campaign have been comprehensively described in Wu et al. (2020). In brief, the CO was measured by a vacuum ultraviolet florescence spectroscopy (AL5002, Aerolaser GmbH, Germany), with an accuracy of 3% and a precision of 1ppby (Gerbig et al., 1999). The refractory black carbon (BC) was characterized using a single particle soot photometer (SP2, Droplet Measurement Technologies, Boulder, CO, USA). The instrument setup, operation and data interpretation procedures can be found elsewhere (McMeeking et al., 2010; Liu et al., 2010). The SP2 incandescence signal was calibrated using Aquadag black carbon particle standards (Aqueous Def locculated Acheson Graphite, manufactured by Acheson Inc., USA), including the correction (0.75) recommended by Laborde et al. (2012a). The overall uncertainty of the BC mass concentration calibration is 20% (Laborde et al., 2012a, b). The chemical compositions of non-refractory submicron aerosols were measured by a compact time-of-flight aerosol mass spectrometer (C-ToF-AMS, Aerodyne Research Inc, Billerica, MA, USA) (Drewnick et al., 2005). Detailed operation of the AMS, including calibration and correction factors, during aircraft deployment has been described previously (Morgan et al., 2009). The AMS was calibrated using monodisperse ammonium nitrate and ammonium sulfate particles. The AMS data were processed using the standard SQUIRREL (SeQUential Igor data RetRiEvaL, v.1.60N) ToF-AMS software package. A time- and composition-dependent collection efficiency was applied to the data based on the algorithm by Middlebrook et al. (2012). The uncertainties of mass concentrations from aircraft AMS are estimated in Bahreini et al. (2009). Figure S2 presents vertical distributions of CO (Fig. S2a) and BC (Fig. S2b) for the CLARIFY flights (C028 to C051). In addition, concurrent surface observations of CO and BC on Ascension Island are also provided in Fig. S2, which presented the same trend of marine boundary layer (MBL) biomass burning (BB) pollution as observed during the CLARIFY campaign (Zuidema et al., 2018). Figure S5 shows vertical profiles of submicron aerosol chemical composition fractions under BBpolluted condition during CLARIFY, which were previously characterized by Wu et al. (2020).

S2 NAME backward-dispersion fields

To investigate the sources and transport pathways of airmasses arriving at Ascension Island, we performed backward-dispersion simulations using the UK Met Office's Numerical Atmospheric Modelling Environment (NAME). Backward-dispersion simulations were performed at 3-hour (h) intervals throughout the campaign period. In each simulation, a certain amount of hypothetical tracer particles (hereafter referred to as "air parcels") (~2.7 × 10⁻⁷ g m⁻³) were released from a 2° × 2° grid box centered around the Ascension Island observation site (7.96°S, 14.35°W). To distinguish source origins of MBL and free troposphere (FT) airmasses over Ascension Island, tracer particles were released within the MBL (341±300 m) and FT (2.5–4 km) altitude ranges separately. NAME backward-dispersion fields can represent the horizontal footprint of air parcels transported over the past 7 days before arriving at the sampling area over Ascension Island. Table S1 summarizes the flight

information and BB pollution conditions in the FT and MBL, for the 17 flights used in this study. For these flights employed in this study, example backward-dispersion fields corresponding to release times within the flight sampling period are presented, distinguishing between FT (Fig. S3) and MBL (Fig. S4) simulations.

35

40

45

50

55

We also employed three case studies to further investigate vertical distributions and the transport of original air parcels for MBL airmasses over Ascension Island. Case 1 released tracers in the middle of Period 1 (12:00 UTC, August 18). Cases 2 and 3 released tracers near the start of Periods 2 (12:00 UTC, August 21) and 3 (12:00 UTC, August 26), respectively, coinciding with shifts in MBL pollution conditions observed over Ascension Island. Case 2 is a reference clean-MBL case for comparison with BB-polluted MBL cases (Cases 1 and 3). For the three case studies, the model output instantaneous 3D air parcel footprints every 3h during the 7-days backward dispersion simulations. We analyzed the instantaneous 3D air parcel footprints in two approaches. First, vertical layers of instantaneous 3D footprints were integrated across the horizontal domain to derive column-integrated horizontal footprints. Instead of using the boundary layer (BL) depth in NAME, the estimated inversion height (z_i) was employed to divide the column-integrated horizontal footprints into the FT and BL separately, distinguishing original air parcels as either from the FT or BL. To present the horizontal transport pattern of air parcels, the instantaneous horizontal fields at each mid-day times are provided for Cases 1 and 3 in Figs. S8 and S9, respectively. The midday step horizontal fields are distinguished between FT and BL sources. Second, horizontal grids were integrated within each vertical layer for instantaneous 3D footprints, to derive vertical distributions of original air parcels as a function of time (at 3h intervals) along the backward simulations. In Fig. S10, we analyzed the vertical distributions of air parcels that were dispersed into the FT region (covering the horizontal area of 20°S - 0°N, 15°W - 12°E) along the backward-simulation time, for two BB-polluted MBL cases. The cumulative exchange amounts of FT air parcels along the backward-simulation time were calculated (black dashed lines in Fig. S10), to indicate the mixing conditions of African air parcels from the FT into the MBL over the southeast Atlantic.

To confirm BB pollution conditions along the simulated transport pathways, we performed a statistical analysis of SEVIRI-retrieved products co-located with NAME instantaneous horizontal fields, at 3-hourly backward step. Here, the SEVIRI-retrieved products include above-cloud aerosol optical thickness (AOT), cloud droplet number concentration (N_d), cloud effective radius (R_e) and cloud-top height (CTH). Examples of the co-location relationship between SEVIRI-retrieved products and NAME instantaneous horizontal footprints are shown in Fig. S11. The parts of the scene that are co-located with the contemporaneous horizontal footprints from NAME simulations are highlighted.

Table S1. Summary of CLARIFY aircraft flights used in this study.

	D.	Take-off	Duration	Pollution	In-cloud	MBL
Flight	Date	time	(hours)	layer (MBL/FT)	period (min)	structure type
C029	17/08/2017	08:56	3:23	MBL	5:38	e
C031	18/08/2017	11:59	3:43	MBL	4:00	d
C032	19/08/2017	10:01	3:43	MBL	33:24	f
C033	22/08/2017	08:54	3:45	FT	7:44	e
C036	24/08/2017	09:03	3:02	FT	23:40	e
C037	24/08/2017	13:46	3:07	FT	1:58	e
C038	25/08/2017	09:00	3:49	MBL&FT	14: 24	e
C039	25/08/2017	14:17	3:06	FT	7: 43	d
C042	28/08/2017	08:55	3:28	MBL&FT	14: 18	e
C044	29/08/2017	08:54	3:50	MBL&FT	36: 34	e
C045	29/08/2017	14:10	3:06	MBL&FT	33:12	e
C046	30/08/2017	08:45	4:06	MBL&FT	11:46	d
C047	01/09/2017	08:56	2:50	MBL&FT	2:21	d
C048	01/09/2017	13:26	3:57	MBL&FT	26:02	e
C049	02/09/2017	08:56	3:43	MBL&FT	11:11	d
C050	04/09/2017	13:28	3:46	MBL&FT	29:47	e
C051	05/09/2017	08:58	3:14	MBL&FT	38:41	d

Note: 1) "MBL" represents marine boundary layer, and "FT" represents free troposphere. 2) "d" represents a decoupled stratocumulus MBL, 3) "e" represents stratocumulus-over-cumulus MBL. 4) "f" represents a cumulus-capped MBL.

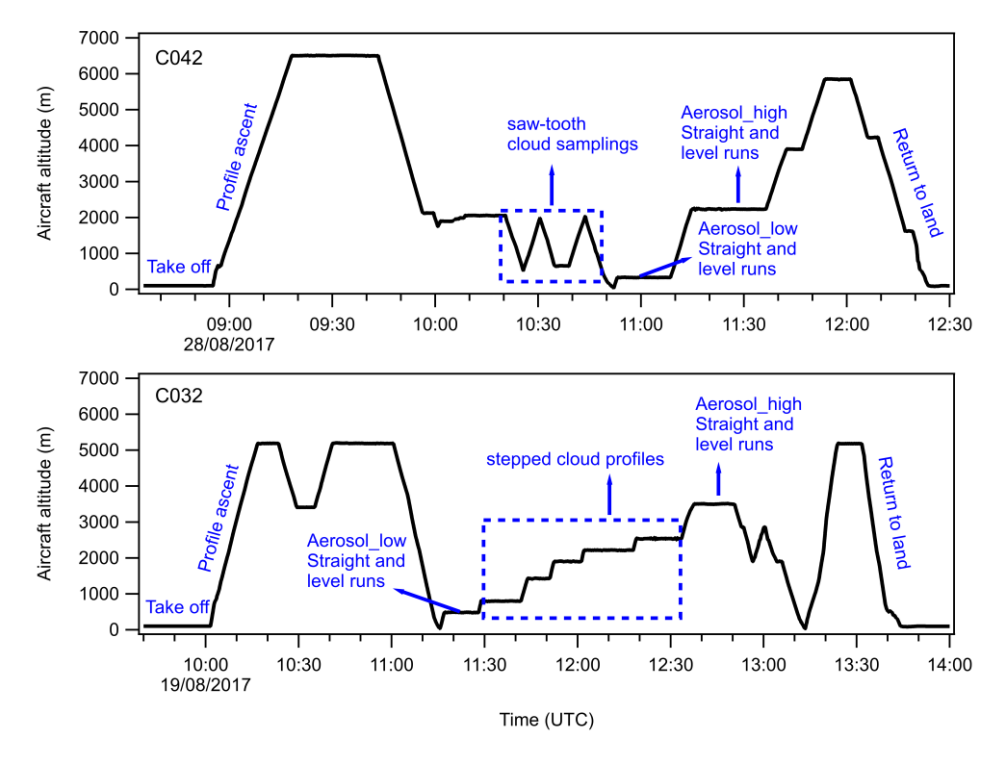


Figure S1. Example flight patterns from flight C042 (top) and C032 (bottom). The example flights provide an illustration of straight and level runs for aerosol characterization and saw-tooth and stepped profiles for cloud samplings.

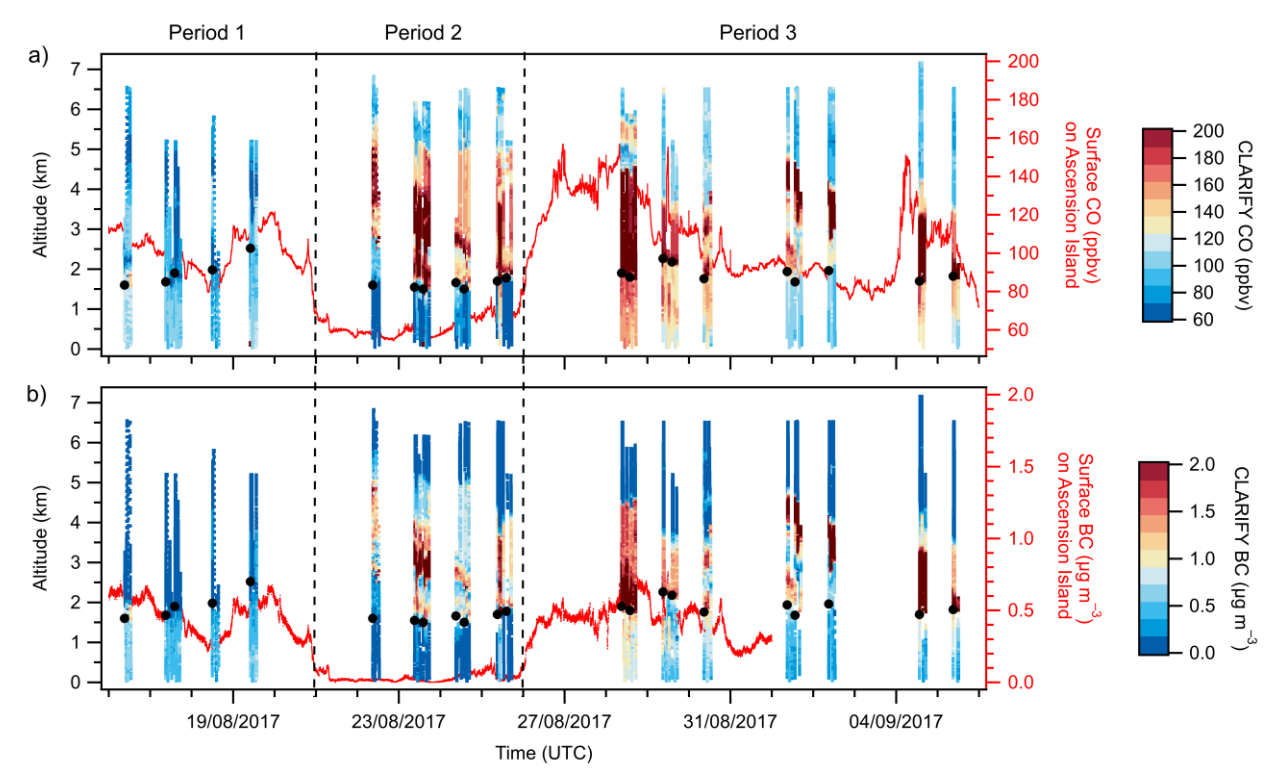


Figure S2. (a) Vertical distributions of CO (ppbv) from the CLARIFY flights (C028 to C051), alongside the estimated z_i from each flight (black circles). The right axis is the surface CO (red line) observed on Ascension Island (Zuidema et al., 2018). (b) Vertical distributions of BC (μ g m⁻³) from the CLARIFY flights (C028 to C051), alongside the estimated z_i from each flight (black circles). The right axis is the surface BC (red line) observed on Ascension Island (Zuidema et al., 2018).

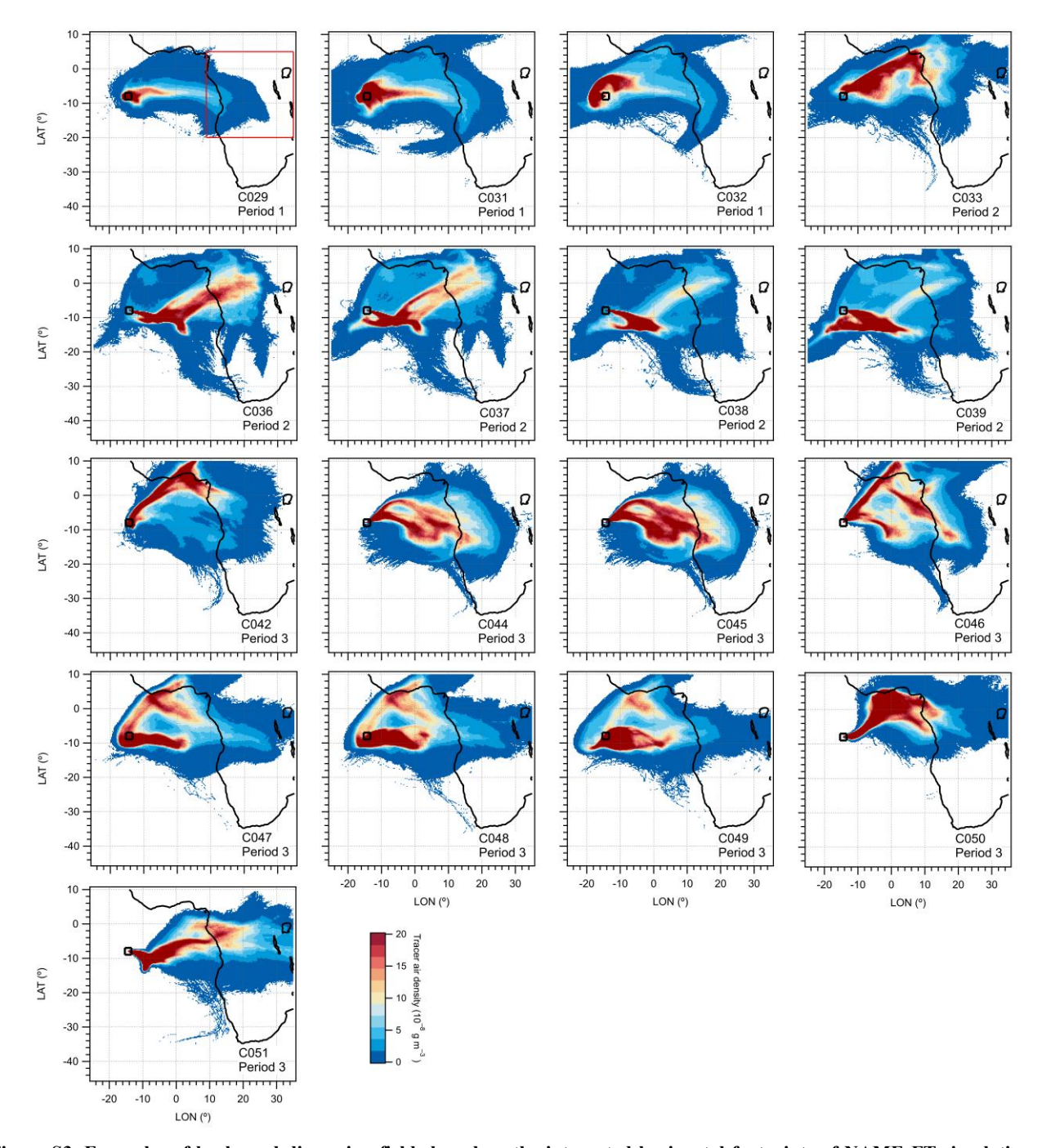


Figure S3. Examples of backward-dispersion fields based on the integrated horizontal footprints of NAME FT simulations. The examples correspond to release times within the sampling periods of the CLARIFY flights used in this study. The flight number and the corresponding classified period are indicated in the lower-right corner of each panel. The red box in the upper-left panel represents the horizontal domain $(20^{\circ}S - 5^{\circ}N, 9^{\circ}E - 35^{\circ}E)$ used for calculating fractional contributions of airmass from the African continent to Ascension Island.

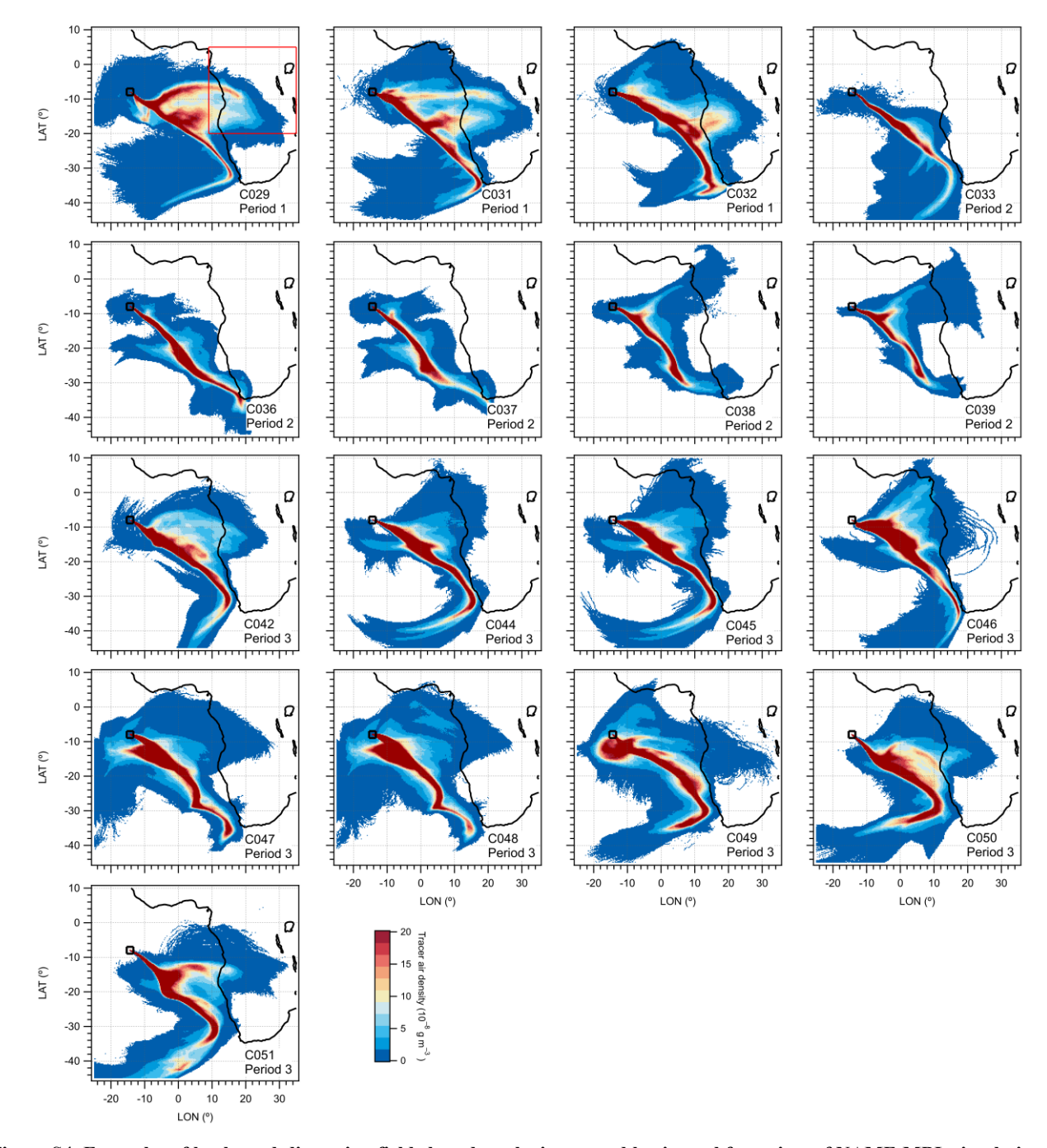


Figure S4. Examples of backward-dispersion fields based on the integrated horizontal footprints of NAME MBL simulations. The examples correspond to release times within the sampling periods of the CLARIFY flights used in this study. The flight number and the corresponding classified period are indicated in the lower-right corner of each panel. The red box in the upper-left panel represents the horizontal domain $(20^{\circ}S - 5^{\circ}N, 9^{\circ}E - 35^{\circ}E)$ used for calculating fractional contributions of airmass from the African continent to Ascension Island.

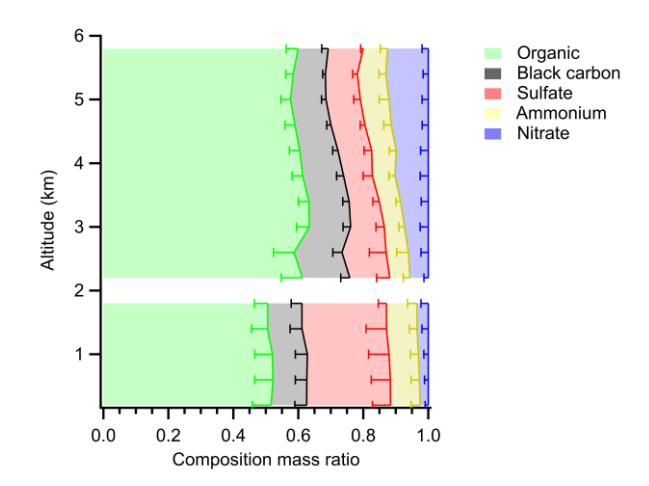


Figure S5. Average vertical profiles of out-of-cloud submicron aerosol chemical composition mass ratios for the flights used in this study, which is modified from Wu et al. (2020). The width of colour bars represents the average mass ratios of different species in each vertical bin. The error bars represent standard deviation.

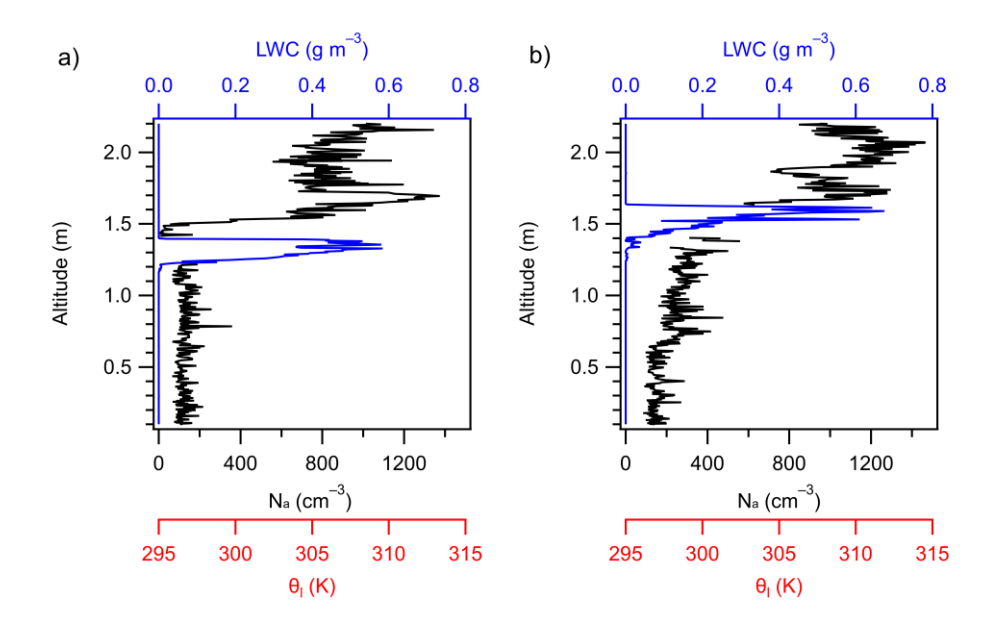


Figure S6. Vertical structures of N_a (black lines), LWC (blue lines), and θ_1 (red lines) in example (a) separate and (b) contact cloud profiles within the clean MBL. (Note: when the distance from the top of the MBL cloud layer to the bottom of the FT BB layer is < 100 m, the cloud profile is defined as a contact profile. The bottom of the FT BB layer is defined as the lowest altitude of the plume where observed N_a exceeded 500 cm⁻³ (Gupta et al., 2021).)

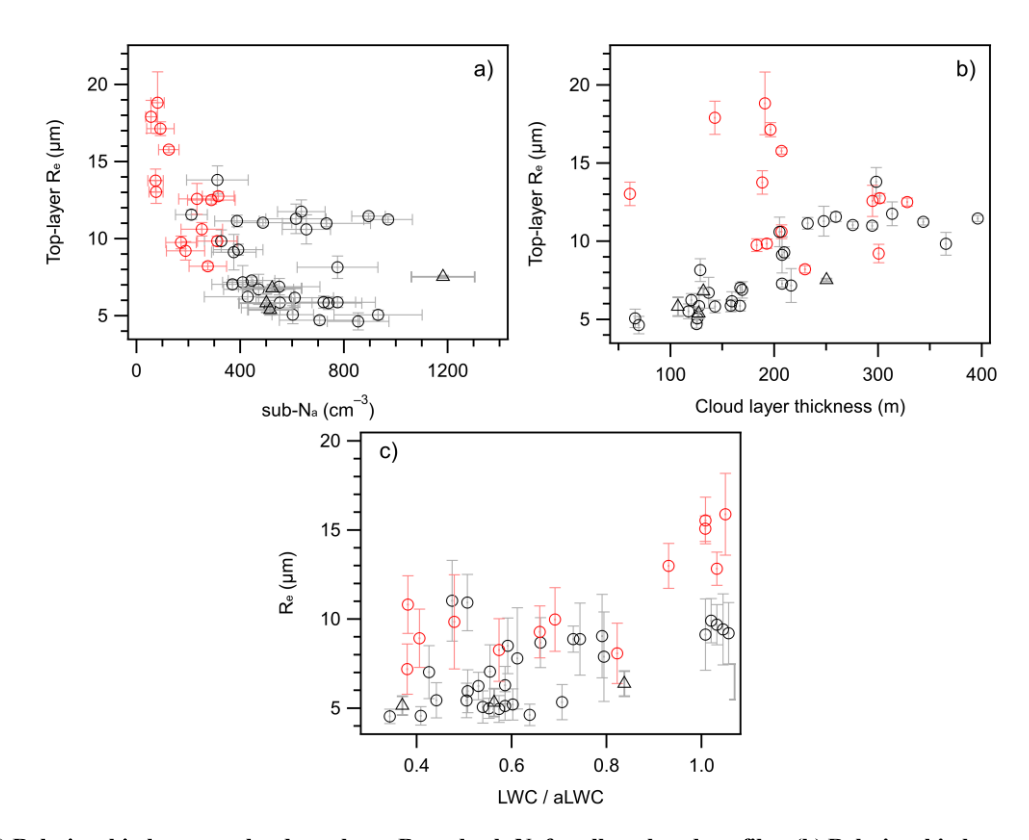


Figure S7. (a) Relationship between cloud-top-layer Re and sub-Na for all analyzed profiles. (b) Relationship between cloud-top-layer Re and cloud layer depth for all analyzed profiles. (c) Relationship between cloud-layer mean Re and the average ratio of LWC/aLWC for all analyzed profiles. The markers and error bars represent the average values and standard deviation for each profile. Black triangle and circle markers are from the BB-polluted MBL in Periods 1 and 3, respectively, and red circle markers are from the clean MBL in Period 2.

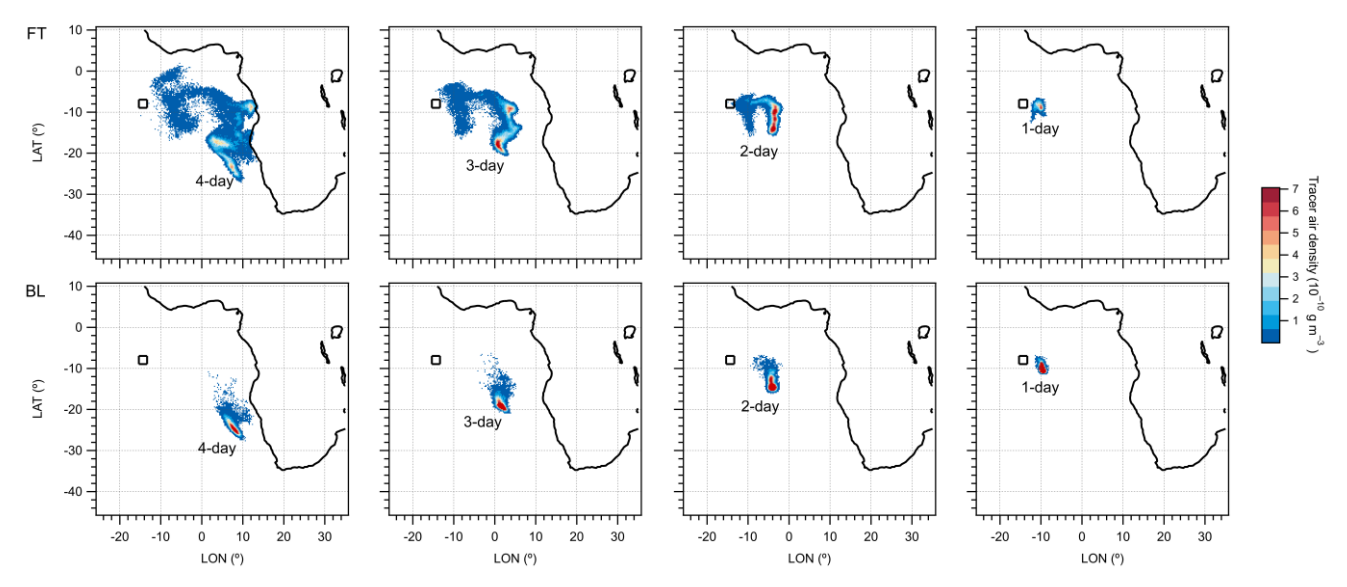


Figure S8. The instantaneous horizontal air parcel fields at each mid-day during 4 days prior to the NAME release time for Case 1 (released from 18 August 2017 at 12:00 UTC). Top panels represent air parcel dispersion results attributed to the FT; bottom panel represent air parcel dispersion results attributed to the BL. From the left to right, the panels indicate the movement of air parcels before arrival at the release location around the Ascension Island area (black box). All panels are shown in same colour scale.

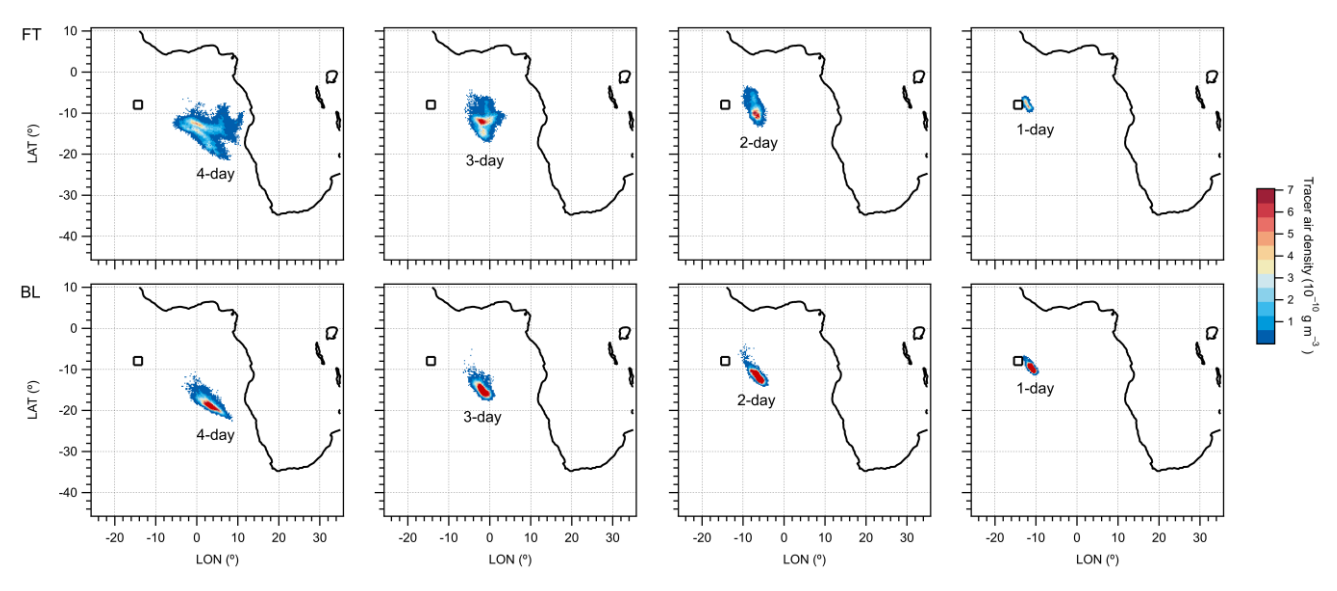


Figure S9. The instantaneous horizontal air parcel fields at each mid-day during 4 days prior to the NAME release time for Case 3 (released from 26 August 2017 at 12:00 UTC). Top panels represent air parcel dispersion results attributed to the FT; bottom panel represent air parcel dispersion results attributed to the BL. From the left to right, the panels indicate the movement of air parcels before arrival at the release location around the Ascension Island area (black box). All panels are shown in same colour scale.

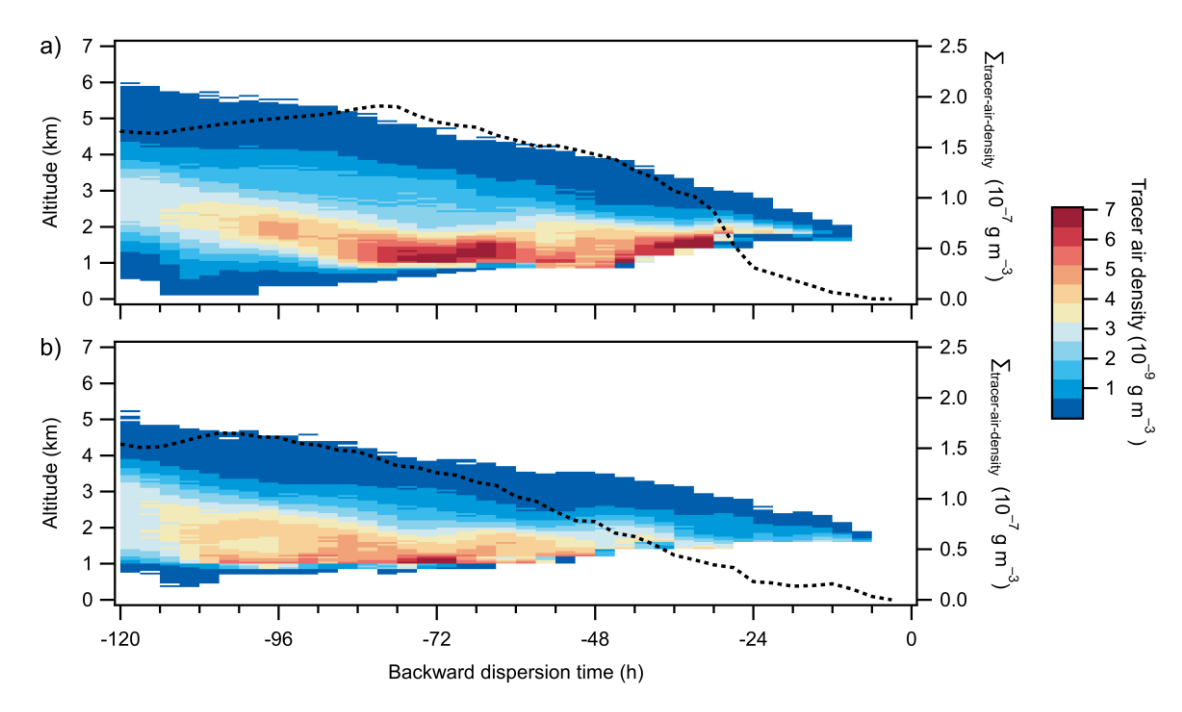


Figure S10. (a-b) Time series of the vertical distributions of air parcels dispersed into the FT region identified in the horizontal area of $20^{\circ}S - 0^{\circ}N$, $15^{\circ}W - 12^{\circ}E$ (see red box in Fig. 8), in terms of backward dispersion time from 3 to 120 h. The right axis (dashed black lines) are the corresponding cumulative exchange amounts of air parcels dispersed between the FT and MBL along backward simulations. (a) is for Case 1 and (b) is for Case 3.

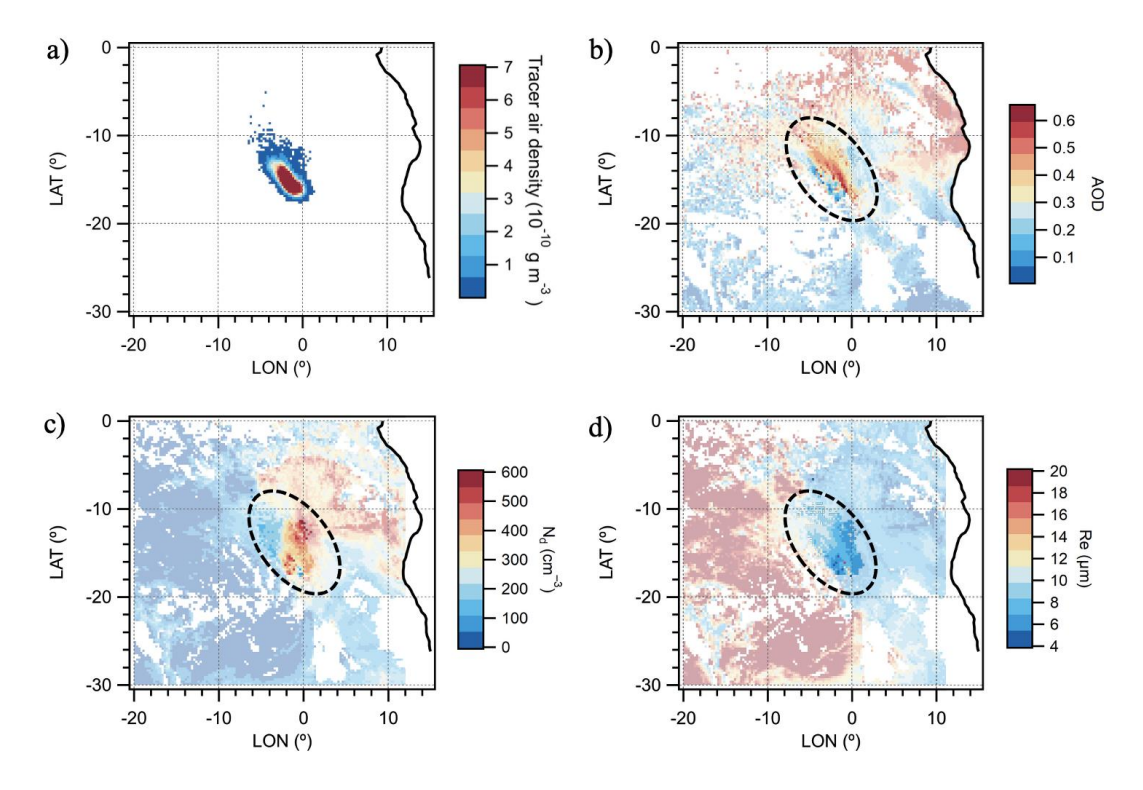


Figure S11. Example co-location relationship between NAME instantaneous horizontal footprints and SEVIRI-retrieved aerosol and cloud fields. (a) is an example BL instantaneous horizontal footprint from NAME simulations. (b-d) are the example SEVIRI-retrieved AOD, N_d and R_e at the time of the example BL horizontal footprint. The parts of the scene (b-d) that are co-located with the contemporaneous horizontal footprints are highlighted. The air-density-weighted average SEVIRI-retrievals were calculated for these co-located areas at 3-hourly backward step.

References

115

120

125

130

Neuman, J. A., Ryerson, T. B., Stark, H., Atlas, E., Brioude, J., Fried, A., Holloway, J. S., Peischl, J., Richter, D., Walega, J., Weibring, P., Wollny, A. G., and Fehsenfeld, F. C.: Organic aerosol formation in urban and industrial plumes near Houston and Dallas, Texas, J. Geophys. Res., 114, D00f16, https://doi.org/10.1029/2008jd011493, 2009.

Drewnick, F., Hings, S. S., DeCarlo, P., Jayne, J. T., Gonin, M., Fuhrer, K., Weimer, S., Jimenez, J. L., Demerjian, K. L., Borrmann, S., and Worsnop, D. R.: A new time-of-flight aerosol mass spectrometer (TOF-AMS)—Instrument description and

Bahreini, R., Ervens, B., Middlebrook, A. M., Warneke, C., de Gouw, J. A., DeCarlo, P. F., Jimenez, J. L., Brock, C. A.,

Gerbig, C., Schmitgen, S., Kley, D., Volz-Thomas, A., Dewey, K., and Haaks, D.: An improved fast-response vacuum-UV resonance fluorescence CO instrument, J. Geophys. Res.-Atmos., 104, 1699–1704, https://doi.org/10.1029/1998JD100031, 1999.

first field deployment, Aerosol Sci. Tech., 39, 637–658, https://doi.org/10.1080/02786820500182040, 2005.

- Gupta, S., McFarquhar, G. M., O'Brien, J. R., Delene, D. J., Poellot, M. R., Dobracki, A., Podolske, J. R., Redemann, J., LeBlanc, S. E., Segal-Rozenhaimer, M., and Pistone, K.: Impact of the variability in vertical separation between biomass burning aerosols and marine stratocumulus on cloud microphysical properties over the Southeast Atlantic, Atmos. Chem. Phys.,
- 21, 4615–4635, https://doi.org/10.5194/acp-21-4615-2021, 2021.
 Laborde, M., Mertes, P., Zieger, P., Dommen, J., Baltensperger, U., and Gysel, M.: Sensitivity of the Single Particle Soot Photometer to different black carbon types, Atmos. Meas. Tech., 5, 10311043, https://doi.org/10.5194/amt-5-1031-2012, 2012a.
 - Laborde, M., Schnaiter, M., Linke, C., Saathoff, H., Naumann, K.H., Möhler, O., Berlenz, S., Wagner, U., Taylor, J. W., Liu,
- D., Flynn, M., Allan, J. D., Coe, H., Heimerl, K., Dahlkötter, F., Weinzierl, B., Wollny, A. G., Zanatta, M., Cozic, J., Laj, P., Hitzenberger, R., Schwarz, J. P., and Gysel, M.: Single Particle Soot Photometer intercomparison at the AIDA chamber, Atmos. Meas. Tech., 5, 3077–3097, https://doi.org/10.5194/amt-5-30772012, 2012b.
 - Liu, D., Flynn, M., Gysel, M., Targino, A., Crawford, I., Bower, K., Choularton, T., Jurányi, Z., Steinbacher, M., Hüglin, C., Curtius, J., Kampus, M., Petzold, A., Weingartner, E., Baltensperger, U., and Coe, H.: Single particle characterization of black
- carbon aerosols at a tropospheric alpine site in Switzerland, Atmos. Chem. Phys., 10, 7389–7407, https://doi.org/10.5194/acp10-7389-2010, 2010.
 - McMeeking, G. R., Hamburger, T., Liu, D., Flynn, M., Morgan, W. T., Northway, M., Highwood, E. J., Krejci, R., Allan, J. D., Minikin, A., and Coe, H.: Black carbon measurements in the boundary layer over western and northern Europe, Atmos. Chem. Phys., 10, 9393–9414, https://doi.org/10.5194/acp10-9393-2010, 2010.
- Middlebrook, A. M., Bahreini, R., Jimenez, J. L., and Canagaratna, M. R.: Evaluation of composition-dependent collection efficiencies for the aerodyne aerosol mass spectrometer using field data, Aerosol Sci. Tech., 46, 258–271, https://doi.org/10.1080/02786826.2011.620041, 2012.
 - Morgan, W. T., Allan, J. D., Bower, K. N., Capes, G., Crosier, J., Williams, P. I., and Coe, H.: Vertical distribution of submicron aerosol chemical composition from North-Western Europe and https://doi.org/10.5194/acp-20-12697-2020 the North-
- East Atlantic, Atmos. Chem. Phys., 9, 5389–5401, https://doi.org/10.5194/acp-9-5389-2009, 2009.
 Wu, H., Taylor, J. W., Szpek, K., Langridge, J. M., Williams, P. I., Flynn, M., Allan, J. D., Abel, S. J., Pitt, J., Cotterell, M. I., Fox, C., Davies, N. W., Haywood, J., and Coe, H.: Vertical variability of the properties of highly aged biomass burning aerosol transported over the southeast Atlantic during CLARIFY-2017, Atmos. Chem. Phys., 20, 12697–12719,

https://doi.org/10.5194/acp-20-12697-2020, 2020.

Zuidema, P., Sedlacek III, A. J., Flynn, C., Springston, S., Delgadillo, R., Zhang, J., Aiken, A. C., Koontz, A., and Muradyan, P.: The Ascension Island Boundary Layer in the Remote Southeast Atlantic is Often Smoky, Geophys. Res. Lett., 45, 4456–4465, https://doi.org/10.1002/2017GL076926, 2018.